Chapter 6

An Overview of Droplet Impact Erosion, Related Theory and Protection Measures in Steam Turbines

Mansoor Ahmad

Additional information is available at the end of the chapter

http://dx.doi.org/10.5772/intechopen.80768

Abstract

Erosion of last-stage steam turbine blades is a well-known problem in the turbine manufacturing industry. Damage of structure and loss of efficiency are the common problems associated with erosion. Understanding of the phenomenon leading to low-pressure blade erosion, erosion protection and erosion prediction has been the topic of scientific research and interest in the steam turbine manufacturing community since the start of the nineteenth century. Although several changes in both the steam turbine stage design and steam properties have been adopted to eliminate this problem, none of them have proved to eradicate this phenomenon completely. The only option left for the scientists and designers is to mitigate the process by utilising materials with high erosion resistance. This requires the development of high erosion-resistive materials and then quantitative confirmation of their erosion resistance by using some precise and accurate laboratory methods reflecting the conditions in the last stage of steam turbines. An overview of droplet impact erosion and related theory has been addressed in this chapter. Moreover, different methods to quantify erosion on a laboratory scale will be presented. In addition, different measures to mitigate erosion in low-pressure stages of steam turbines will be described. In the end, different droplet impact erosion prediction approaches will be discussed.

Keywords: droplet impact, shock wave, water hammer, jetting, erosion

1. Introduction

Erosion of steam turbine blades was first recognised by the turbine manufacturing industry at the start of the nineteenth century when the velocities of the rotating blades of steam turbines became sufficient to cause erosion. At that time, the erosion of steam turbine blades by

different possible phenomena including chemical attack, oxidation and solid particles carried by the steam was tried to be explained (Coles 1904) [1]. However by the 1920s, experimental studies focusing on the erosion of steam turbine blades by droplet impact had been started [2]. In 1928, Cook presented his water hammer equation in which he estimated the pressure generated when a liquid column impacts on a solid surface. In his theory, he proved that the pressure generated at the liquid-solid impact is sufficient to exceed the yield strength of many steel alloys typically used for steam turbine blades [1]. The following section aims to highlight the phenomenon of liquid-solid impact and to provide a brief review of the scientific findings and developments in this field.

2. Liquid-solid impact

Liquid-solid impact is important in many engineering and industrial applications like the erosion of turbine blades due to high-speed impacts of condensed droplets in the expanding steam, cavitation damage in hydraulic components, erosion of aircraft wings due to the impact of rain droplets, erosion of soil due to rain droplets and impacts of water waves on river banks and erosion of embankments on the seashore.

The impingement of a liquid on a solid in the form of a jet or high-speed droplet was analysed by Joukowski in 1898, who first described the importance of compression waves in the liquid, mentioning the formation of high pressures arising on the liquid-solid impact. In 1928, Cook recognised the same concept in the form of his water hammer equation. In his theory, he explained the high pressure on liquid-solid impact by the formation of compression waves in the liquid taking into account the compressibility of the liquid. He proved that the water hammer pressure is many times higher than the steady pressure of a jet at the same velocity. He related it to the pressure P_{impact} arising from the compressible nature of impacting liquid also known as the water hammer equation:

$$P_{impact} = \rho_l C_l V_{impact} \tag{1}$$

where ρ_l is the mass density of the liquid; C_l is the acoustic speed in the liquid, which, with some limitations, represents the speed of shock wave propagation in it; and V_{impact} is the impact velocity [3]. This equation plays an important role in this work as it provides a means of scaling the impact pressure with impact velocity.

As illustrated by **Figures 1** and **2**, when a liquid droplet with a curved surface approaches a solid surface, then at the first instant of impact, the contact area increases with a velocity greater than the shock wave speed in the liquid. The exact value of this velocity depends upon the radius of the droplet and the velocity with which the droplet approaches the surface. So in the initial regime, the contact edge spreads out with a velocity greater than that of the shock wave, and the liquid is compressed within the shock envelope giving maximum pressure at the impact surface. This maximum pressure reduces to static pressure when the shock envelope overtakes the contact edge and release waves can enter the liquid. The contact region

http://dx.doi.org/10.5772/intechopen.80768

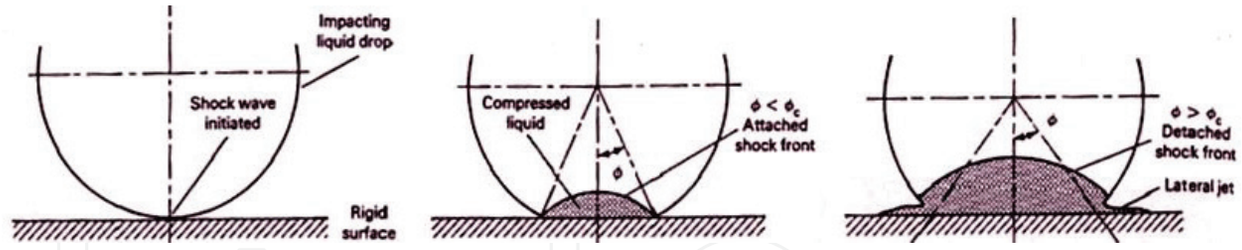

Figure 1. Idealised diagram of early stages of liquid drop impact. From Heymann [4].

over which the compressed shock envelope occurred is given by radius $R_{contact}$, which is of the order of rV_{impact}/C_l (r is the radius of droplet), whereas the time taken to complete this radius is $rV_{impact}/2Cl^2$. As release waves take an extra time of rV_{impact}/Cl^2, so the compressed nature of the flow will occur for the total time of $3rVi_{mpact}/2Cl^2$ [1].

The liquid-solid interaction is further complicated when the solid surface becomes deformed from erosion, usually exhibiting peaks and craters. For example, a drop falling on a peak or slope may not develop the full impact pressure, and on falling in a crater, it may produce increased pressure due to shock wave collisions [4].

The formation of the shock envelope was explained by Lesser in 1981 using the Huygens principle. As shown in **Figure 3**, in the initial regime, when the contact edge velocity is greater than that of a shock wave, at each instant the expanding liquid edge will emit an expanding wavelet moving with acoustic velocity C_l. So at each instant, the liquid will consist of two zones, one with expanding wavelets and another outside the wavelets where liquid is still not affected by impact. In the initial regime, the droplet edge will coincide with these wavelets and form the shock envelope. In the second regime (**Figure 4**), when the edge velocity is lower than the shock speed, the wavelet travels up to the free edge of the droplet, and the compressed liquid trapped in the shock envelope flows away laterally [5].

The geometrical acoustic model from Lesser gives the detailed pressure distribution field inside the impacting drop [5, 6]. According to the model, the pressure at the centre of the impact is the water hammer pressure of $\rho_l C_l V_{impact}$; there are even higher pressures at the expanding droplet contact edge. This high pressure at the contact edge attains a maximum

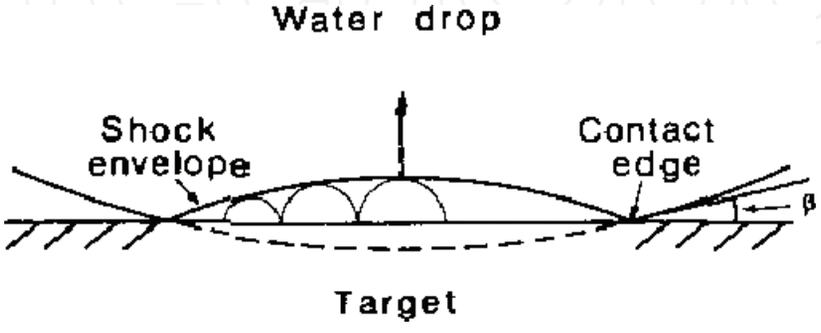

Figure 2. Initial regime of droplet impact on surface with contact edge velocity higher than shock wave speed. The liquid is compressed in the shock envelope giving the maximum pressure. The shock envelope is composed by many wavelets. From Field [1].

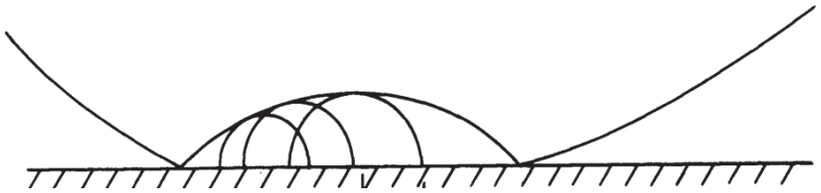

Figure 3. Impact of droplet on a surface and subsequent Huygens wavelet construction forming shock envelope separating disturbed and undisturbed liquid. From Lesser [5].

value of $3\rho_l C_l V_{impact}$ just before the shock envelope overtakes the contact edge. The reason for this high pressure is the bunching of the wavelets at the contact edge as the contact edge velocity deceases. This high pressure of $3\rho_l C_l V_{impact}$ at the contact edge lasts only for a short duration of time and has a very small effect on the surface damage as compared to the sustained damage caused by the $\rho_l C_l V_{impact}$ pressure.

The pressure field under the liquid impact was investigated experimentally by Rochester and Brunton (1974) and Rochester (1979) who recorded the pressure distribution using piezoelectric ceramic gauges embedded in the impact surface. The ratio of edge-to-central pressures was about 2.8, which is quite close to the theoretical estimations [1].

2.1. Jetting angle and time

The angle at which jetting starts was given by Bowden and Field in 1964 by the relations:

$$\beta_c = Sin^{-1}(M_i) \tag{2}$$

where M_i is the impact Mach number based on the liquid speed of sound and velocity for impact with a rigid target. The time at which jetting starts and at which the pressure reaches its maximum value is given by the relation:

$$T_j = \frac{rV_{impact}}{2C_l^2} \tag{3}$$

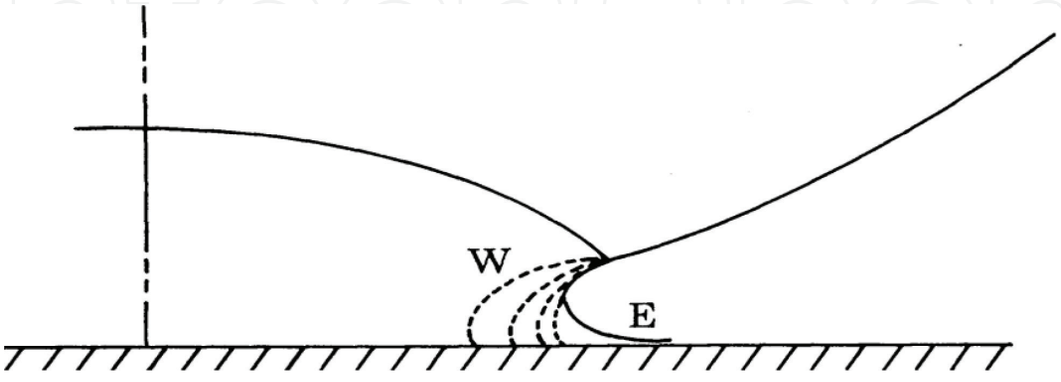

Figure 4. The second regime in the liquid droplet impact when the edge velocity is lower than the shock wave velocity. The expanding wavelet travels up to the free edge of the liquid, and the trapped liquid is released away in the form of lateral jetting. From Lesser [5].

http://dx.doi.org/10.5772/intechopen.80768

where r is the radius of the droplet. However, experimental studies found even greater angles and hence greater jetting times than those predicted by theory. Hancox and Brunton explained this by the effects of viscosity, which delays the onset of jetting [7]. However, this explanation was not logical due to the high pressures and velocities involved in this phenomenon. Lesser [5] suggested that the deformability of the target has a major effect on increasing the jetting angle β_c. Experiments, conducted by Field et al. in 1985 using steel and PMMA as the target surfaces, confirmed the Lesser theory that target admittance has a major effect on the critical angle at which jetting commences [8]. However, this delay in jetting is too small to explain the completely different jetting times obtained by theory and experiments. Lesser and Field [6] tackled the problem in a different way. According to their theory, as the shock wave travels upwards, the liquid particles would be ejected by the release wave in a direction perpendicular to the local droplet surface (**Figure 5**). In this way, paths of ejected liquid particles would cross each other. They argued that during the initial stage of droplet impact, the edge angle β is very small, and the gap between the droplet surface and impact surface would practically be closed by the jet of ejected liquid particles and hence cannot be detected [8]. Using this theory to explain the delay in jetting, Field et al. (1988) suggested two values of β; β_c and β_j, where βc is the angle at which the shock wave overtakes the contact edge and starts to spall liquid into the air gap and βj is the angle at which this spalled liquid moves ahead of the contact edge and can be observed as a jet [6].

2.2. Impact pressure

Impact pressure on a solid surface upon the collision of a droplet is given by the water hammer pressure as $\rho_l C_l V_{impact}$. Here ρ_l is the mass density of the liquid, C_l is the speed of shock wave propagation in it and V_{impact} is the impact velocity [3]. In 1933, de Haller pointed out that this pressure is valid only when the impacting surface is rigid [9]. In the case of a compressible solid, the resulting pressure would be

$$P_{impact} = \frac{\rho_l C_l V_{impact}}{1 + \frac{\rho_l C_l}{\rho_s C_s}} \tag{4}$$

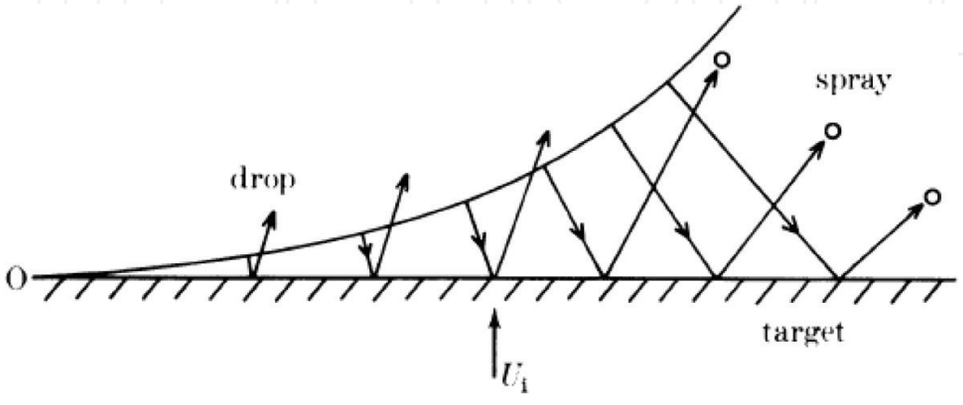

Figure 5. Trajectories of liquid particles upon the impact of a droplet. From Lesser and Field [6].

where subscripts l and s denote liquid and solid, respectively. In the water hammer equation, its descendants and the Lesser acoustic model 1981, the shock speed has been approximated by the acoustic speed of the liquid itself. However, Heymann in 1968 [10] explained that this approximation is valid only for the lower-impact speed regimes and if impact speed exceeds certain limits, then this simple relation does not hold anymore. In his model, he argued that the impact pressure is not uniform along the impact line. While the pressure at the centre of impact is water hammer pressure, there are even higher pressures found at the contact edge. The pressure at the contact edge increases gradually as the contact perimeter grows with time, while the pressure at the impact centre deceases. The maximum pressure found at the contact edge is up to three times the water hammer pressure at the moment of shock wave lifting up the droplet free surface. For higher-impact velocities, the impact pressure can be approximated by seeking the dependence of shock wave speed on particle speed change across the shock front as;

$$P_{impact} = \rho_l C_l V_{impact}. \left(1 + \frac{kV_{impact}}{C_l}\right) \tag{5}$$

The value of *K* is found to be 2 for water. So if a water drop impacts on a solid surface with an impact speed of 500 m/s, the impact pressure would be 1250 MPa, considerably above the yield strength of many alloys.

2.3. Shock wave speed

The water hammer equation $\rho_l C_l V_{impact}$ has been derived from momentum considerations using an idealised case where the parameters are assumed to be invariant. This approximation is valid for relatively lower-impact velocities where the shock wave speed C can be reasonably approximated by the acoustic velocity of the liquid C_l. However in the case of high-speed liquid impact, the compressibility can be taken into account in the variation of density ρ_l and/or shock wave speed C, and the water hammer pressure is needed to correct for the mass transport across the shock front due to compressibility.

Heymann [10] proposed an approximate relationship for water for the shock wave velocity C as a function of particle velocity change ΔU as follows:

$$C = C_l + K\Delta U \tag{6}$$

where C_l is ambient speed of sound and ΔU is the liquid particle velocity change across the shock front. K is some constant, and with the help of experimental data, he found K = 2 for water. This equation is limited for Mach number Mi < 1.2. Actually K is not a constant, and for very large Mach numbers, K approaches unity as $k = \rho/(\rho - \rho_o)$, where ρ is the density in the compressed state. The value of particle velocity change across the shock front during the initial regime of the impact is found to be equal to the impact velocity [11]. Haller also observed the same effect when he numerically calculated the shock wave speed by considering a 100 μm droplet impacting on a solid surface with an impact speed of 500 m/s. Within the first stage of impact where the shock wave is still in contact with the contact edge, he found

http://dx.doi.org/10.5772/intechopen.80768

a shock speed in the range of 2600–3000 m/s, which is substantially higher than the ambient speed of sound in water [12]. By using the same conditions as used by Haller, the shock speed calculated by Heymann's Eq. (6) comes out to be 2500 m/s.

2.4. Jetting velocity

Jetting occurs when the critical angle is reached, and the shock travels up the free surface of the drop. Bowden and Brunton (1961) suggested a relationship between the jetting angle and jetting speed as follows:

$$Vj = V_{impact} \operatorname{Cot}\left(\frac{\beta}{2}\right) \tag{7}$$

where V_j is the jetting velocity and β is the jetting angle. Field et al. found that provided $\beta > \beta c$, the jetting velocity is greater for smaller values of β. The particles that form jetting first travel normally to the drop surface and towards the target surface. They also cross each other's path on rebound, and the particles which travel closest to the target surface are those which are ejected later. In certain impact speed ranges, the jetting velocity is found to be up to 10 times the impact velocity [8]. This is further verified by Field et al. (1989) by high-speed photography. Haller (2002) numerically found that the jetting velocity of up to 6000 m/s can be obtained for a 100-μm droplet impacting on a surface with impact speed of 500 m/s. By using the same conditions as used by Haller and using Eqs. (2) and (7), the jetting velocity comes out to be 3000 m/s.

2.5. Cavitation

Field et al. [8] observed that when a droplet impacts on a solid target, then after the initial regime with a high-pressure zone in the centre of impact, expansion waves come from the free surface and jetting commences (**Figure 6**). These expansion waves have the same magnitude as the compression waves, and the liquid is brought back to the initial ambient conditions. These expansion waves cross each other and bring the liquid into negative pressure and cause cavitation. These cavities collapse near the solid surface, produce both shocks and microjets, add pressure near the solid surface and contribute to the damage of the target surface [8]. Haller (2002) numerically studied the formation of cavitation during the impact of a 100-μm droplet on a solid surface with an impact speed of 500 m/s (**Figure 7**). His picture of droplet impact shows that after lifting up the droplet free surface, the shock wave reflects normally to the droplet free surface as expansion waves. These expansion waves create cavitation in the middle of the drop. Contrary to the cavitation picture given by Field in 1985, expansion waves in Haller's simulations are focused only in the middle of a drop and have no significant effect on the damage of the surface. However, Rein reported that upon the droplet impact, cavitation fields can be observed above the interface between the target surface and the liquid as well as below the apex of droplet. However, only the cavitation formed at the interface is well known for severe erosion [13].

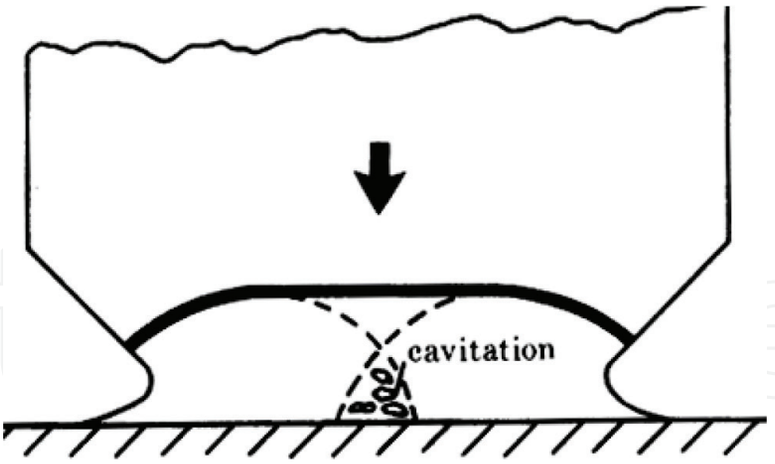

Figure 6. Formation of cavitation at the impact of a jet on a solid surface. From Field et al. [8].

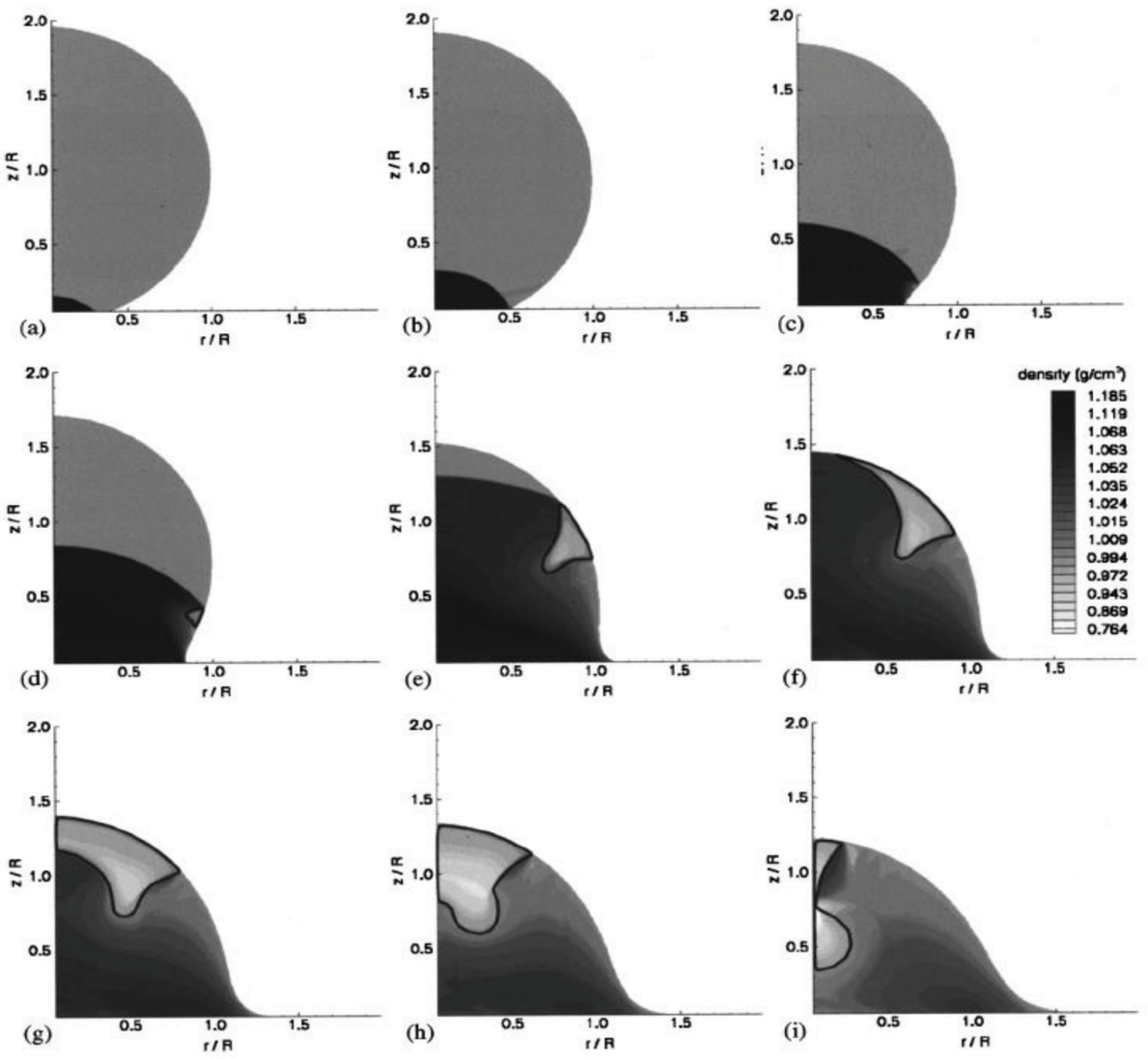

Figure 7. Formation of shock wave in a liquid droplet upon impact on a solid surface. From Haller et al [12].

http://dx.doi.org/10.5772/intechopen.80768

3. Droplet impact erosion

Thomas and Brunton [14] investigated repeated liquid impacts for several materials. Erosion curves are drawn for each material and then generalised into one curve, which shows the presence of three stages (**Figure 8**). The first stage is the incubation period during which no weight loss occurred, but some plastic or brittle deformation was noted. In stage 2, pits formed and grew by the removal of material. In stage 3, the erosion rate fell down to a lower value. The growth of small depressions (stage 1) into pits was explained by the stress concentrations. Even though the average stress is low, local soft points of materials may account for yielding. At the start, these local disturbances are very rare, so the first depression would appear with some delay. Later on, with the formation of many depressions, the erosion rate would arise. In stage 2, the tangential flow over the roughened surface also greatly influences the erosion phenomenon; work hardening and eventual fracture of the material occur. In stage 3, the rate of erosion declines again since the drop is broken up by the roughened surface; also the impact is no longer normal to the surface. They tried to compare the constant erosion damage with the fatigue mechanism.

3.1. Time dependence of erosion rate

With less intense but repeated impacts, there is no immediate material loss, but randomly disposed dimples gradually develop, and the surface undergoes gradual deformation and work hardening. The material loss may occur through the propagation of fatigue-like cracks that intersect to release erosion fragments. In materials with non-uniform structure, damage will initiate at weak spots. In brittle materials, circumferential cracks may form around the impact site, which are caused by the tensile stress waves propagating outwards along the surface [4].

Heymann (1969) [4] characterised the repetitive impact erosion in five different stages (**Figure 9**) as follows:

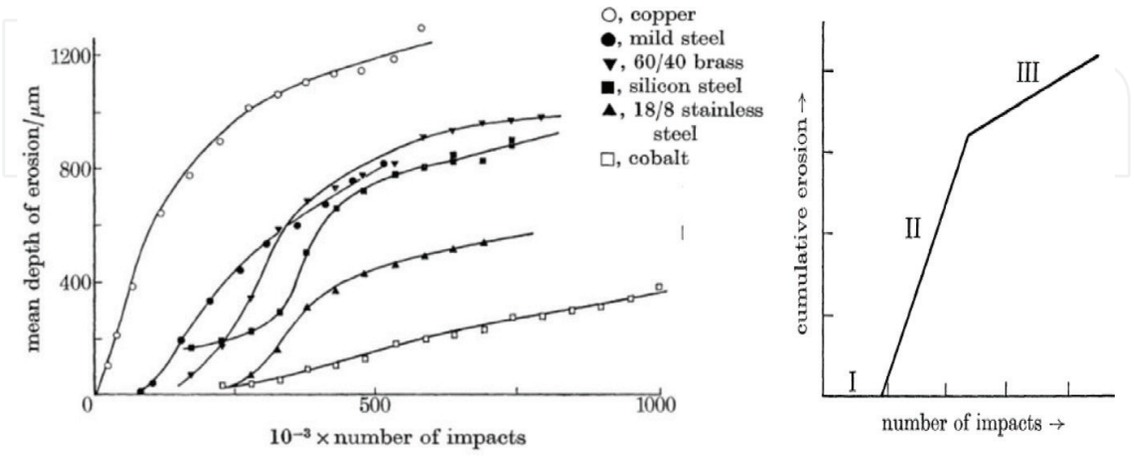

Figure 8. The development of erosion in a number of materials eroded at an impact velocity of 125 m/s with a water jet diameter of 1.5 mm. (a) Experiment results and (b) three-stage model for erosion process. From Thomas and Brunton [14].

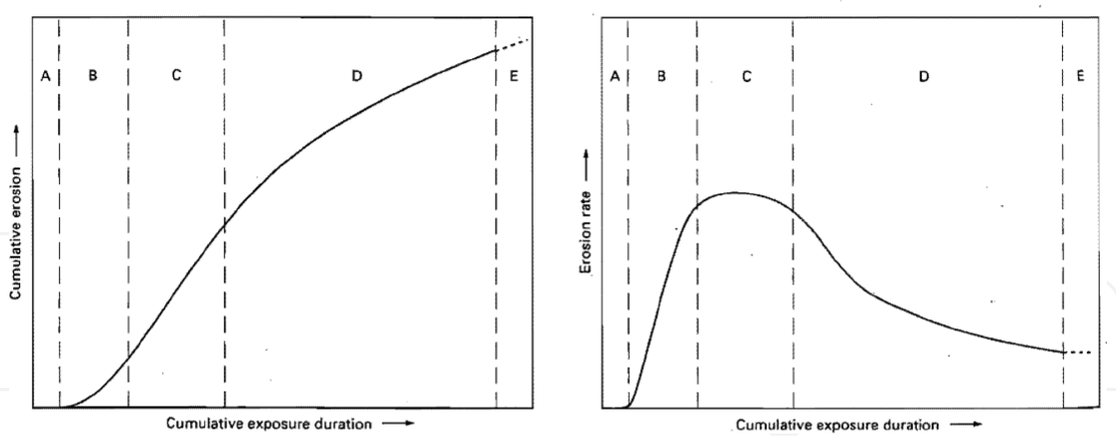

Figure 9. Characteristic erosion versus time curves. (A) Incubation stage, (B) acceleration stage, (C) maximum rate stage, (D) deceleration stage and (E) terminal stage. From Heymann (1969).

3.2. Incubation stage A

During this stage, little or no material loss occurs, although roughening and metallurgical changes take place in the surface. However, the incubation period may not occur if the impact conditions are severe enough.

3.3. Acceleration stage B

During this stage, the erosion rate increases rapidly to a maximum value. The extent of this maximum erosion rate depends mainly upon the erosive environment and the material erosion resistance.

3.4. Maximum rate stage C

During this stage, the erosion rate remains constant or nearly so. The continuous material removal from the cumulated pits forms the constant peak of this erosion stage.

3.5. Deceleration stage D

During this stage, the erosion rate declines to some fraction of the maximum rate (1/2–1/4).

3.6. Terminal stage E

During this stage, the erosion rate remains constant once again indefinitely. However, some tests do not show this stage.

3.7. Reasons for time dependence

The incubation and acceleration stages are easy to explain if it is assumed that the erosion results from a fatigue-like failure mechanism. Then many impacts must occur in one area for a fragment

http://dx.doi.org/10.5772/intechopen.80768

to be loosened, and we have a gradual transition—the acceleration period—from the incubation period to the maximum rate stage. The subsequent decrease in erosion rate is explained by different concepts. Some relate it to the increase in surface area after the surface has roughened, so the more energy is needed to remove the material. Some relate it to the fact that on the eroded surface, peaks and craters tend to decrease the erosion rate as drops falling on the peaks or slopes will result in decrease in impact pressure. Also the liquid retained in the craters is supposed to cushion the impact. Some relate it to the work hardening of the eroded surface [4].

3.8. Factors affecting erosion

Erosion can be characterised by its fundamental driving parameters, which help to provide insight into the governing phenomenon. In the following paragraphs, these fundamental parameters have been classified in different groups, and their influences on erosion have been summarised.

3.9. Impingement parameters

3.9.1. Impact velocity

Many authors give the idea of threshold velocity dependent on the material and also on the droplet size below which no erosion would take place, analogous to the endurance limit in fatigue. However at low-impact velocities, the incubation period becomes so long that no material loss takes place in a reasonable testing time, which may give the appearance of a threshold so this phenomenon is not yet firmly settled. Dependence of erosion on impact velocity can be explained by the simple power law as Erosion~V^n where n is found to be in the range of 4–5. For brittle materials, exponents as high as 6–9 have been reported [4, 15].

3.9.2. Impact angle

Except for any scouring action, erosion depends only on the normal component of the impact velocity; thus, because of the strong dependence on the impact velocity, erosion is reduced strongly as the impacts become more glancing. However, when the surface is roughened by erosion, the effect of the tangential component is more pronounced [4, 15].

3.9.3. Droplet size

Ahmad et al. [16] proved experimentally that the erosion of low-pressure steam turbine blades increases with the impacting droplet size. In other words, erosion tends to reduce as the drop size decreases, that is, a given volume of water did less damage if divided into smaller drops even though it implies more impacts on the surface. This is probably due to the fact that in fatigue, the spatial extent of imposed stresses must exceed some characteristic dimension [4]. They showed that the influence of droplet size on the extent of erosion can be presented by a simple power law relation Erosion~D^n_{impact}. They found the value of n in the range of 3.2–3.5 for the common steam turbine blade materials [16]. If the effect of droplet size is combined with that of impact speed, the scale of steam turbine blade erosion may significantly be changed.

3.10. Dependence on liquid properties

Most liquid impact erosion tests have been performed with water at normal atmospheric conditions. However, some tests have been performed with different liquid properties, which show that the erosion varies with approximately the 2nd to 2.5th power of liquid density and the 1/2–3/4 power of the inverse of viscosity. Moreover, a slight increase in erosion is found by an increase in the impacting liquid temperature. This mechanism is explained by the increased shear damage of the target surface, which is caused by the resulting lateral jet flow [4].

3.11. Correlation with mechanical properties

It is always desirable to correlate erosion resistance of materials with a single mechanical property. It is found that hardness, resilience, toughness, tensile strength, ductility and the strain energy can affect erosion resistance greatly, but comprehensive knowledge is not yet available in this field [4, 14, 15, 17, 18]. Moreover, a ductile material with more toughness is more erosion resistant. Also annealed materials show greater erosion resistance than the cold-worked materials [14].

3.12. Effects of alloying elements and microstructure

Improved erosion resistance has been associated with alloying elements such as chromium, manganese and cobalt. The effect of nickel is inconsistent. Fine microstructure is advantageous and so is the ability of the surface layer to become work-hardened as a result of impact-induced deformation. The extremely high erosion resistance of Stellite (cobalt-chromium-tungsten alloy) has been explained by a microstructure consisting of small hard carbide particles in a strong but more ductile matrix. Very high erosion resistance has been reported for chromium-manganese steels (about 10% Cr and 12% Mn) that undergo austenitic-martensitic phase transformation under impingement. Simoneau et al. found that low stacking-fault energy is the key to high erosion resistance in austenitic stainless steel as well as cobalt base alloys [4, 15].

4. Steam turbine blade erosion

In the last stages of low-pressure steam turbines, the steam expands to well below saturation conditions, and a portion of the vapour condenses into liquid. Although the condensation droplets are very small (5–10 μm), some of them are deposited on the surfaces of the stationary blades (guide vanes), where they coalesce into films and migrate to the trailing edge. Here they are torn off by the steam flow, in the form of much larger droplets. In the wake between stator and rotor, these large droplets slowly accelerate under the aerodynamic forces of the steam. However, when these large droplets enter the plane of rotation of upcoming rotating blades, they have gained only a fraction of the steam velocity. As a result of the difference in steam and droplet absolute velocities, the droplets collide with the rotating blades

with a velocity that is almost equal to the circumferential velocity of the blades. In a modern 3600 rpm turbine, the impact speed is estimated to be as high as 700 m/s [15, 19].

4.1. Quantification of droplet impact erosion

Since the recognition of the erosion phenomenon in the low-pressure stages of steam turbines, many experiments have been designed to study the erosion phenomenon on laboratory scale by simulating the conditions as observed in a real steam turbine. Worthington (1908) was the first who studied liquid-solid impact experimentally by using high-speed photography. The first study about erosion was carried out in a Parsons steam turbine plant in 1925. Honneger [2], Gardner (1932) and de Haller [9] were the pioneers in the experimental study of steam turbine blade erosion. The basic methodology to simulate the droplet impact erosion on a laboratory scale is to arrange a high-speed droplet impact on a target surface. This high-speed droplet impact is, typically, achieved in a rotating test rig where the specimen alone or the specimen and nozzle both rotate in a controlled environment to achieve a predesigned impact speed and number impacts on the target surface [15, 20]. Some scientists achieved this high-speed droplet impact by using some special arrangements where they used a chamber that is closed at the one end by a piston and at the other end by the specimen surface. By operating on the piston, a high-speed jet or a shock wave is produced, which subsequently impacts on the target surface [14, 21].

The materials, which are to be tested in the test rig to find out their erosion resistance, are milled in a cylindrical, rectangular or a button-like shape [15]. Ahmad et al. performed the experiments with blade-like specimens. These specimens experience similar impact angles and impact speeds on their surfaces in the erosion rig as those observed for the corresponding blade spans in the real steam turbine, whereby the erosion process is accelerated by increasing the droplet impact number [22].

The test duration is normally motivated by the test intent specification to greatly accelerate the erosion process in such a way that monotonic saturating material loss gradients can be established within a feasible time frame. To quantify the erosion, the weight loss is interpreted with the help of the material density to reflect the volumetric erosion of the material. As a second key figure, the area-specific first-time derivative, i.e. the erosion rate, is derived and evaluated. As the erosion rate reflects the tendency of a material to erode at a given erosive environment, its reciprocal value will reflect the resistivity of the material to erode in terms of time taken by the erosive environment for a given degree of material degradation [15].

4.2. Protection against droplet impact erosion

As soon as the phenomenon causing the droplet impact erosion has been well understood and agreed amongst the scientific community, different remedial measures have been proposed and implemented to avoid the erosion of steam turbine blades. In the first step, the axial spacing between stator and rotor has been increased. In an increased path between stator and rotor, the droplets are further accelerated and broken up into smaller droplets under the action of steam aerodynamic forces. Moreover, trailing edges of the stator guide vanes are deliberately made thinner. This leads to smaller initial secondary droplets produced from

the water film at the trailing edges. To reduce the number of droplets impacting the rotating blades, the moisture in the last stages of steam turbines was extracted. This was achieved by providing suction slots on the stator surface. Moreover, the stationary guide vanes were heated up to evaporate the water film developed on the guide vane surface. However, amongst all, heating up the stationary guide vanes is proved to be the most efficient erosion remedial cure [23, 24].

If materials are tested at a laboratory scale where erosive environment can be kept as constant as possible, then materials classification can be established on the basis of measured surface degradation. If tested for a constant time period, this process leads to the determination of relative material erosion resistance. Using this criterion, titanium is found to have more erosion resistance than the steel alloys of the same or even greater hardness. As the erosion starts and intensifies on the blade leading edges, it is ensured that the blade leading edges are particularly more resistant against droplet impact erosion. The erosion resistance of blade leading edges has been improved by different case-hardening methods, which include laser treatments, induction or flame-hardening as well as shot peening of the blade materials. Moreover, blade leading edges have been shielded with Stellite and tool steel to protect the base metal against erosion [4, 15, 24]. Laser gas nitriding can effectively be used to increase the erosion resistance of titanium materials [20, 25, 26]. On the other hand, shot peening as well as the laser shock peening is found to be ineffective. Stellite 6B is found to be the best choice for steel blade shielding, whereas beta titanium alloy has more or less the same erosion resistance as that of Stellite 6B [27].

4.3. Prediction of droplet impact erosion

After understanding the mechanism leading to droplet impact erosion, quantifying the erosion on laboratory scale and proposing different erosion mitigation measures, the scientists, then, tried to predict droplet impact erosion in steam turbine blades. This idea gained popularity as the prediction of the erosion of low-pressure steam turbine blades eventually helps in the prediction of the service life of turbines. Different empirical and theoretical theories have been suggested and proposed to predict the droplet impact erosion. However, these prediction theories only worked for some specific materials and turbine environments. If the blade materials and/or impacting droplet parameters were changed, these theories completely failed to predict the droplet impact erosion. It should be noted that the erosion of steam turbine blading is a function of different steam, liquid and material properties and these properties may also depend upon each other. These dependencies make the prediction of steam turbine blade erosion more and more complicated. In real life, the operating conditions of the individual steam turbines are not constant, which makes the prediction of erosion a challenge for the researchers working on this topic [28–31].

The prediction of steam turbine blade erosion is a direct measure of the erosion resistance and behaviour of the concerned material in response to a given erosive environment. Taking into account the above fact, a normalised erosion resistance has been proposed. This normalised erosion resistance is defined as "the volume loss rate of a test material, divided by the volume loss rate of a specified reference material similarly tested and similarly analysed". In different occasions, austenitic stainless steel (170 HV hardness), stainless steel (type 308) and some other

materials have been used as reference materials [4]. This idea could gain popularity if the same reference material was tested worldwide in a similar test rig under the same testing conditions.

Similarly some theoretical parameters have been proposed to define the erosion resistance of materials [32]. However, these parameters cannot be used to predict the erosion resistance of materials mainly due to the difficulty to evaluate these parameters. Sometimes these parameters even failed to verify the empirically observed results and dependencies.

In another approach, droplet impact erosion phenomenon has been correlated with material fatigue mechanism; see, e.g. [7, 14]. According to this theory, as both erosion and fatigue are triggered by the repeated stress pulses, therefore both processes can be similarly analysed and tackled. However, the idea to correlate droplet impact erosion with fatigue is not exclusively agreed and understood within the scientific community. On the other hand, some authors tried to correlate the erosion resistance of a material on its surface microstructure. Similarly, interatomic bond strength and the size and distribution of surface flaws have been tried to define the erosion resistance of the concerned material [7]. Although hardness is used universally to assess the erosion resistance of a material, resilience and toughness are the parameters, which also gain consideration and importance in the scientific community [15, 33–35].

5. Summary

The erosion of last-stage steam turbine blades is a subproblem within the domain of steam condensation in the low-pressure stages of steam turbines. The slowly accelerating secondary droplets, detached from the trailing edges of the guide vanes, eventually hit the following rotating blades with an impact speed, which is mostly determined by the blade circumferential speed. The droplets impact on the suction side of the blade mainly due to the droplet impact velocity relative to the moving blades. The position of droplet impact on the blade, axial penetration of the droplets and their angle of impact are largely influenced by the droplet absolute velocity, its size and initial boundary as well as the flow conditions.

Upon a droplet impact, the material degradation is mainly triggered by the impact shock pressure and subsequent lateral jetting. The impact shock pressure is largely influenced by the compressive nature of the flow and subsequent shock wave generation in the compressed liquid. The shock wave speed is not invariant and depends upon the droplet impact velocity and impacting medium. Using water as an impacting medium, a droplet with an impact speed of 500 m/s may produce a shock pressure on the target surface, which is up to 10 times greater than the corresponding stagnation pressure and exceeds the yield strength of many steel alloys. Although the intensity of impact shock pressure seems to be independent of impacting droplet size, its duration and the impacted area depend upon the droplet size. The other deteriorating agent, i.e. lateral jetting, having the speed of several times the impact velocity, becomes important when the surface is composed of several discontinuities. These discontinuities might already be pre-existent on the surface or are the results of erosion itself.

The erosion can be related to the impact velocity by a power law equation of the type $f(x) = kx^n$. The value of n basically depends upon the type of material. It is found that for

ductile materials, n varies from 3 to 5, whereas for brittle materials, values as high as 7 are observed. Erosion is found to be an angle-dependent process where the perpendicular impact plays the dominant role. The dependence of erosion on impact angle can be explained by the dependence of erosion on impact speed, if it is assumed that the erosion proceeds with the normal component of impact velocity only. Among others, impacting droplet size is a key parameter contributing to the erosion of low-pressure steam turbine blades. It is also found that volume loss per droplet impact increases with droplet size with a simple power law relation $Erosion \sim D^{n}_{droplet}$, where value of n is found to be 3.2 up to 3.5 for common blade materials.

Erosion is found to be a time-dependent process, which eventually leads to a saturation stage. An eroded blade sustains most of its life under this saturation stage. The intensity of saturating period and the initiation of saturation depend upon the erosive environment harshness as well as the material properties. Most important is that the eroded surface undergoes several changes during the erosion process and eventually tends to enter a stable regime, which is then characterised by the saturation of erosion as well as the eroded surface structure.

The erosion resistance of a material can be presented by its physical as well as mechanical properties. Within materials having the same metallurgical structure, the erosion resistance increases with the surface hardness. When comparing materials having different metallurgical structures, the other material properties are required to explain the relative material erosion resistance. Hardness-induced elastic resilience and toughness are found to be effective parameters when materials from different groups are compared.

Prediction of erosion is interesting in many aspects as it may serve for the prediction of next blade repair work as well as helping to understand the basic erosion phenomenon. The prediction of erosion may be accomplished once the erosion strength of the target surface is explicitly defined and understood. Being a function of several independent variables, the problem of erosion prediction can be examined by introducing appropriate dimensionless numbers.

Author details

Mansoor Ahmad

Address all correspondence to: mabbwp@gmail.com

Institute of Thermal Turbomachinery and Machinery Laboratory (ITSM), University of Stuttgart, Germany

References

[1] Field JE. The physics of liquid impact, shock wave interactions with cavities, and the implications to shock wave lithotripsy. Physics in Medicine and Biology. 1991;**36**(11):1475-1484

[2] Honegger E, Ueber den Verschleiß von Dampfturbinenschaufeln, BBC Mitteilungen. 1927

[3] Cook SS. Erosion by water hammer. Proceedings of the Royal Society of London. 1928;**119**(783):481-488

[4] Heymann FJ. Liquid impingement erosion. In: ASM Handbook: Friction, Lubrication, and Wear Technology. Vol. 18. Material Park, Ohio, USA: ASM International; 1992. pp. 221-232

[5] Lesser MB. Analytic solutions of liquid drop impact problems. Proceedings of the Royal Society of London. 1981;**377**(1730):289-308

[6] Lesser MB, Field JE. The impact of compressible liquids. Annual Review of Fluid Mechanics. 1983;**15**:97-122

[7] Hancox NL, Brunton JH. The erosion of solids by the repeated impact of liquid droplets. Proceedings of the Royal Society of London. Series A: Mathematical and Physical Sciences. 1966;**260**(1110):121-139

[8] Field JE, Lesser MB, Dear JP. Studies of two-dimensional liquid-wedge impact and their relevance to liquid-drop impact problems. Proceedings of the Royal Society of London. 1985;**401**(1821):225-249

[9] de Haller P. Unsuchungen über die durch Kavitation hervorgerufnen Korrosionen. Schweizerische Bauzeitung. 1933;**101**:243-246

[10] Heymann FJ. On the shock wave velocity and impact pressure in high speed liquid-solid impact. Transactions of the ASME. Series D, Journal of Basic Engineering. 1968;**90**:400-402

[11] Huang YC, Hammitt FG, Mitchell TM. Note on shock-wave velocity in high-speed liquid-solid impact. Journal of Applied Physics. 1973;**44**:1868-1869

[12] Haller KK, Ventikos Y, Poulikakos D. Computational study of high-speed liquid droplet impact. Journal of Applied Physics. 2002;**92**:2821-2828

[13] Rein M. Phenomena of liquid drop impact on solid and liquid surfaces. Fluid Dynamics Research. 1993;**12**(2):61-93

[14] Thomas GP, Brunton JH. Drop impingement erosion of metals. Proceedings of the Royal Society of London. 1970;**314**(1519):549-565

[15] Ahmad M, Casey M, Sürken N. Experimental assessment of droplet impact erosion resistance of steam turbine blade materials. Wear. 2009;**267**(9-10):1605-1618

[16] Ahmad M, Schatz M, Casey M. Experimental investigation of droplet size influence on low pressure steam turbine blade erosion. Wear. 2013;**303**(1-2):83-86

[17] Smith A, Caldwell J, Pearson D, McAllister DH, Christie DG. Physical aspects of blade erosion by wet steam in turbines. Philosophical Transactions of the Royal Society of London. Series A, Mathematical and Physical Sciences. 1966;**260**(1110):209-219

[18] Fujisawa N et al. The influence of material hardness on liquid droplet impingement erosion. Nuclear Engineering and Design. 2015;**288**:27-34

[19] Ilieva G. Mechanisms of water droplets deposition on turbine blade surfaces and erosion wear effects. Journal of Applied Fluid Mechanics. 2017;**10**(2):551-567

[20] Mahdipoor MS, Kevorkov D, Jedrzejowski P, Medraj M. Water droplet erosion behaviour of gas nitrided Ti6Al4V. Surface and Coatings Technology. 2016;**292**:78-89

[21] Bowden FP, Brunton JH. The deformation of solids by liquid impact by supersonic speeds. Proceedings of the Royal Society of London. 1961;**263**(1315):433-450

[22] Ahmad M, Sigg R, Casey M, Sürken N. Steam turbine blade erosion assessment using specimens with a blade-like profile. In: Proceedings of the 8th European Turbomachinery Conference. Graz, Austria; 2009. pp. 1125-1136

[23] Schwerdtner OAv, Hosenfeld H-G. Developments for the prevention of blade erosion in low pressure end stages. VGB PowerTech. 1977;**57**(4):217-226

[24] Akhtar MS, Black J, Swainston MJC. Prevention of steam turbine blade erosion using stator blade heating. Proceedings of the Institution of Mechanical Engineers. 1977;**191**(1): 355-361

[25] Batory D, Szymanski W, Panjan M, Zabeida O, Klemberg-Sapieha JE. Plasma nitriding of Ti6Al4V alloy for improved water erosion resistance. Wear. 2017;**374-375**:120-127

[26] Kamkar N, Bridier F, Bocher P, Jedrzejowski P. Water droplet erosion mechanisms in rolled Ti–6Al–4V. Wear. 2013;**301**(1-2):442-448

[27] Ahmad M. Experimental Assessment of Droplet Impact Erosion of Low-Pressure Steam Turbine Blades. Germany: Shaker Verlag Aachen; 2009, ISBN 978-3-8322-8603-3

[28] Krzyzanowski JA, Kowalski AE, Shubenko AL. Some aspects of erosion prediction of steam turbine balding. Transactions of the ASME. 1994;**116**:442-451

[29] Ruml Z, Straka F. A new model for steam turbine blade materials erosion. Wear. 1995;**186-187**:421-424

[30] Mack R, Drtina P, Lang E. Numerical prediction of erosion on guide vanes and in labyrinth seal in hydraulic turbines. Wear. 1999;**233-235**:685-691

[31] Lee B-E, Riu K-J, Shin S-H, Kwon S-B. Development of a water droplet erosion model for large steam turbine blades. KSME International Journal. 2003;**17**(1):114-121

[32] Springer GS. Erosion by Liquid Impact. New Jersey, United States: John Wiley & Sons; 1976

[33] Klaestrup Kristensen J, Hansson I, Mørch KA. A simple model for cavitation erosion of metals. Journal of Physics D: Applied Physics. 1978;**11**:899-912

[34] Atkins T. Toughness and processes of material removal. Wear. 2009;**267**(11):1764-1771

[35] Ahmad M, Schatz M, Casey MV. An empirical approach to predict droplet impact erosion in low-pressure stages of steam turbines. Wear. 2018;**402-403**:57-63